Quasi-Freestanding Graphene on SiC(0001) by Ar-Mediated Intercalation of Antimony: A Route Toward Intercalation of High-Vapor-Pressure Elements

*Susanne Wolff, Sarah Roscher, Felix Timmermann, Marcus V. Daniel, Florian Speck, Martina Wanke, Manfred Albrecht, and Thomas Seyller**

A novel strategy for the intercalation of antimony (Sb) under the $(6\sqrt{3} \times 6\sqrt{3})R\,30°$ reconstruction, also known as buffer layer, on SiC(0001) is reported. Using X-ray photoelectron spectroscopy, low-energy electron diffraction, and angle-resolved photoelectron spectroscopy, it is demonstrated that, while the intercalation of the volatile Sb is not possible by annealing the Sb-coated buffer layer in ultrahigh vacuum, it can be achieved by annealing the sample in an atmosphere of Ar, which suppresses Sb desorption. The intercalation leads to a decoupling of the buffer layer from the SiC(0001) surface and the formation of quasi-freestanding graphene. The intercalation process paves the way for future studies of the formation of quasi-freestanding graphene by intercalation of high-vapor-pressure elements, which are not accessible by previously known intercalation techniques, and thus provides new avenues for the manipulation of epitaxial graphene on SiC.

1. Introduction

Since the ground-breaking work of Novoselov and Geim[1] graphene has been in the focus of numerous scientists. Of special importance was and still is the development of optimized processes for the controlled large-scale production of graphene. A possible route toward graphene-based electronics was proposed by the group of Berger and de Heer,[2,3] who suggested to employ high-temperature graphitization of silicon carbide (SiC) to produce so-called epitaxial graphene. This technique, which is frequently referred to as sublimation growth, relies on the fact that SiC decomposes at the surface at temperatures above ≈1200 °C, leading to sublimation of volatile Si atoms leaving behind C atoms which condense into graphitic layers.[4] The advantage of epitaxial graphene on SiC is that it can be made on a wafer scale on an insulating substrate so that it can be patterned and processed without the necessity of a transfer. Consequently, epitaxial graphene on SiC has evolved into a very active field.[5] A major breakthrough in this area of research was the development of sublimation growth in argon (Ar) atmosphere[6,7] which led to an improved homogeneity of epitaxial graphene on SiC(0001). More recently, a further improvement of the structural quality of graphene on SiC(0001) was obtained by the so-called polymer assisted sublimation growth.[8] Epitaxial graphene grown on SiC holds much promise for applications, for example, in quantum metrology[9] or high-frequency transistors[10–12] and researchers have devised methods for manipulating its properties, in particular, by intercalation of different elements.

In order to understand this, basics of the growth and some structural aspects should be recalled. On the Si-terminated SiC(0001) surface, epitaxial graphene grows in an ordered fashion, where the lattice vectors are aligned with an angle of 30° with respect to the basal plane lattice vectors of the substrate. The epitaxial relationship is maintained by the presence of the so-called buffer layer, which is a carbon layer with $(6\sqrt{3} \times 6\sqrt{3})R\,30°$ periodicity ($6\sqrt{3}$ for short) and which is topologically identical to graphene. This buffer layer is strongly coupled to the SiC surface such that it lacks the typical π bands of graphene.[13,14] A schematic representation is given in **Figure 1**a. The buffer layer is formed in the early stages of the growth process which can be stopped in order to obtain a SiC(0001) surface covered only with the buffer layer. However, if the sublimation process is continued, a new buffer layer is formed at the interface by

S. Wolff, S. Roscher, F. Timmermann, Dr. M. V. Daniel, Dr. F. Speck, Dr. M. Wanke, Prof. M. Albrecht, Prof. T. Seyller
Institute of Physics, Faculty of Natural Sciences, TU Chemnitz
09107 Chemnitz, Germany
E-mail: thomas.seyller@physik.tu-chemnitz.de

S. Roscher
Fraunhofer Institute for Applied Solid State Physics
79108 Freiburg, Germany

F. Timmermann, Prof. M. Albrecht
Institute of Physics
Faculty of Mathematics, Natural Sciences, and Materials Engineering
University of Augsburg
86135 Augsburg, Germany

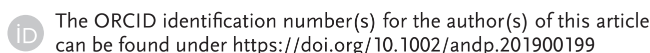
The ORCID identification number(s) for the author(s) of this article can be found under https://doi.org/10.1002/andp.201900199

© 2019 The Authors. Published by WILEY-VCH Verlag GmbH & Co. KGaA, Weinheim. This is an open access article under the terms of the Creative Commons Attribution License, which permits use, distribution and reproduction in any medium, provided the original work is properly cited.

The copyright line for this article was change on September 26, 2019 after original publication online.

DOI: 10.1002/andp.201900199

 © 2019 The Authors. Published by WILEY-VCH Verlag GmbH & Co. KGaA, Weinheim

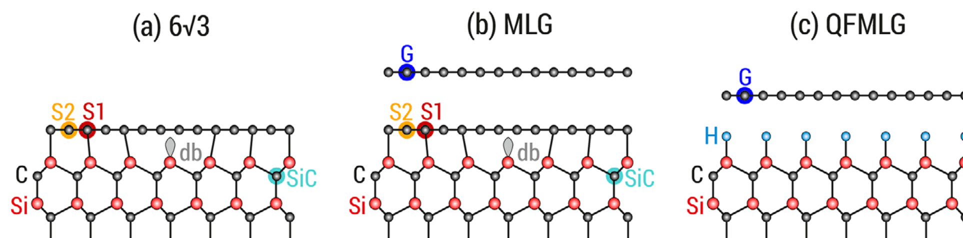

Figure 1. a–c) Schematic representation of the structure (side view) of: a) the buffer layer ($6\sqrt{3}$), b) monolayer graphene (MLG) on the buffer layer, and c) quasi-freestanding graphene (QFMLG) obtained by hydrogen intercalation. The label "db" stands for dangling bond. The labels "S1", "S2", and "SiC" in (a,b), and "G" in (b,c) refer to the components observed in the C1s core level spectra discussed further below. Drawing not to scale.

out-diffusion of Si. The previous buffer layer loses its strong coupling to the substrate and becomes graphene (called monolayer graphene or MLG in the following), thereby sitting on top of the new buffer layer,[14,15] as is shown schematically also in Figure 1b. The registry between the buffer layer and the SiC(0001) surface is thus responsible for the above mentioned epitaxial relationship.[14] Previous experiments have shown, that the buffer layer has consequences for the electronic properties of MLG. It induces an n-type doping with a density of excess electrons of $n \approx 1 \times 10^{13}$ cm^{-2} leading to a position of the Dirac energy E_D around 450 meV below the Fermi level E_F.[16–18] Furthermore, it is responsible for the strong temperature dependence of the charge carrier mobility.[19] Several studies have shown that it is possible to convert the buffer layer into so-called quasi-freestanding monolayer graphene (QFMLG) by intercalation. In this process, a certain element (intercalant) is inserted between the SiC(0001) substrate and the buffer layer. The strong interaction between the SiC(0001) surface and the buffer layer is then lifted and the buffer layer converts into graphene with its typical, linear π bands. Figure 1c schematically depicts the structure of QFMLG for the case of hydrogen intercalation. Note, that by using the same scheme it is also possible to convert MLG (graphene on the buffer layer) into quasi-freestanding bilayer graphene (QFBLG) which shows corresponding parabolic π bands at the K point.

A wide variety of elements has been intercalated and it was observed that the resulting QFMLG layers exhibit different properties including different doping levels, electronic structures (e.g., minicones), and transport properties, depending on the chemical nature and amount of the intercalant, as discussed in the studies listed below. Hence it is interesting to extend such intercalation studies to previously unexplored elements. In their seminal work, Riedl and co-workers[20] demonstrated the intercalation of hydrogen (H) by annealing in H_2 atmosphere. The intercalation of oxygen (O) by annealing in molecular O_2 was shown by Oida et al.[21]. Other groups have investigated the intercalation of oxygen by annealing in air[22,23] in order to produce QFBLG on an oxidized SiC surface. In addition to the elements hydrogen and oxygen, which are normally present in the gas phase, solid elements like gold (Au),[24] copper (Cu),[25] and germanium (Ge)[26] have also been intercalated. This can be achieved by deposition of ultrathin layers of up to a few monlayers of the intercalant on top of the buffer layer at room temperature followed by annealing in ultrahigh vacuum (UHV) to a temperature high enough to enable diffusion of the intercalant to the interface but low enough to prevent its desorption. Typical temperatures are several hundred degree celsius. On the other hand, the intercalation of bismuth (Bi) had to be performed in a different manner due to the volatile nature of Bi which vanished completely from the surface during the annealing step which works so well in the case of Au, Cu, or Ge. In order to achieve the intercalation of Bi, Stöhr et al.[27] employed low-energy ion implantation of Bi into the surface region of a $6\sqrt{3}$ sample followed by annealing at 700 °C. Although this method is promising for intercalation of volatile solid elements under the buffer layer, it also requires the use of specialized tools which are not widely available. In addition, radiation damage was observed.[27] Defects in the QFMLG had to be repaired by annealing in methane (CH_4). Hence another method to intercalate solid elements with high vapor pressure would be of great interest. Here, we recollect the advantage of the Ar atmosphere during the growth of graphene on SiC: it slows down Si desorption so that higher temperatures can be employed to grow graphene with an improved surface morphology.[6] This suggests that an Ar atmosphere could act as a diffusion barrier for volatile atoms such that they stay long enough on the surface for successful intercalation. To test this hypothesis we have investigated the intercalation of antimony (Sb) by annealing in Ar.

2. Experimental Section

Nitrogen-doped 6H-SiC(0001) purchased from *SiCrystal* was used as a substrate for the growth of the $6\sqrt{3}$ samples. Prior to the growth, the substrate surface was etched in hydrogen.[28] The $6\sqrt{3}$ structure was obtained by annealing in Ar at a pressure of $p = 1$ bar and a temperature of $T = 1475$ °C for $t = 15$ min in a furnace described in detail elsewhere.[28] Sb was deposited on the $6\sqrt{3}$ samples by molecular beam epitaxy (MBE) in a separate system using a calibrated Sb Knudsen cell. During the deposition of Sb, the pressure in the MBE chamber was maintained at or below 1×10^{-9} mbar. Note, that after Sb deposition the samples had to be transported in air. Hence an oxidation of the Sb layers at the surface has to be expected. Consequently, either 50 nm or 250 nm of Sb were deposited.

For intercalation, the samples were annealed at different temperatures as described in more detail further below. In first and unsuccessful experiments, the Sb covered $6\sqrt{3}$ samples were annealed in situ in the analysis chamber under UHV conditions. Ex-situ annealing under Ar was carried out in a furnace virtually identical to that used for the growth of $6\sqrt{3}$ and graphene in Ar.[28] The Ar pressure was 1 bar and the temperatures varied between 400 °C and 550 °C as discussed below.

© 2019 The Authors. Published by WILEY-VCH Verlag GmbH & Co. KGaA, Weinheim

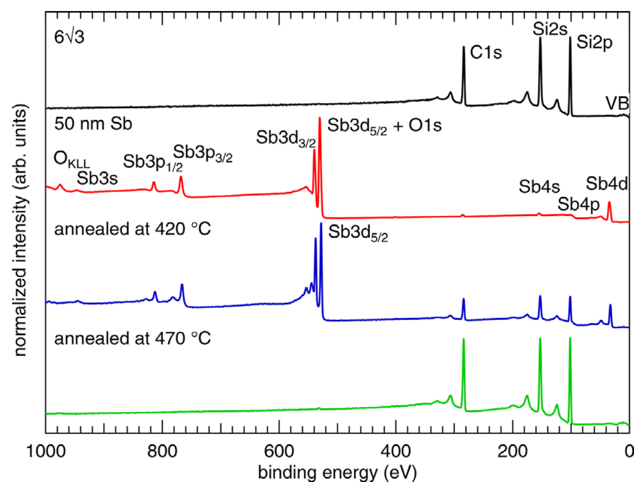

Figure 2. XPS survey spectra of (from top to bottom) a pristine $6\sqrt{3}$ sample, the $6\sqrt{3}$ sample covered with 50 nm Sb and transported in air, the Sb-covered sample after subsequent annealing in UHV at 420 °C and at 470 °C. Spectra are offset from each other for clarity and normalized to the highest peak.

The results of the different preparation steps were characterized by X-ray photoelectron spectroscopy (XPS) using monochromatized Al K_α radiation provided by a Specs XR 50 X-ray source in conjunction with a Specs Focus 500 monochromator and a Specs Phoibos 150-MCD9 analyser. Selected samples were also characterized by angle-resolved photoelectron spectroscopy (ARPES) using a Specs UVS 300 He-lamp in combination with a Specs TMM304 monochromator and a Specs Phoibos 150 analyser with a 2D-CCD-detector. ARPES measurements were performed with HeII radiation. Furthermore, low-energy electron diffraction (LEED) was employed to investigate the samples. Prior to these measurements, the intercalated samples were allowed to degas in UHV by mild annealing to about $T = 300\,^\circ$C.

3. Results and Discussion

At this point, we briefly discuss the unsuccessful attempt to intercalate Sb by annealing the Sb covered $6\sqrt{3}$ sample in UHV, a procedure which was shown to work for, for example, Au,[24] Cu,[25] and Ge.[26] **Figure 2** shows XPS survey spectra (taken with a pass energy of $E_p = 50$ eV) after the individual process steps. The spectrum of the $6\sqrt{3}$ sample before Sb deposition (topmost spectrum) shows signals due to Si (Si2p at $E_b \approx 101$ eV and Si2s at $E_b \approx 152$ eV) and C (C1s at $E_b \approx 284$ eV). The latter includes the carbon atoms in the SiC substrate as well as those forming the buffer layer. Broader and smaller peaks at higher binding energies as the core levels can be attributed to plasmon losses (PL) of the SiC substrate.

The spectrum after deposition of 50 nm Sb (second spectrum from top) shows signals due to the Sb overlayer. The most prominent lines (from lowest to highest binding energy) are the Sb4d line at $E_b \approx 32$ eV, where the spin orbit doublet is not resolved, the Sb3d line, which is split into the $Sb3d_{5/2}$ at $E_b \approx 530$ eV and $Sb3d_{3/2}$ with $E_b \approx 539$ eV components, as well as the $Sb3p_{3/2}$ ($E_b \approx 768$ eV) and $Sb3p_{1/2}$ ($E_b \approx 813$ eV) lines. Looking at the two spin-orbit-split $Sb3d_{5/2}$ and $Sb3d_{3/2}$ components one notices, especially in comparison to the third spectrum, an unexpected intensity ratio where the $Sb3d_{5/2}$ line appears too intense. This is caused by the fact that this line is overlapped by the O1s core level, which has a binding energy of ≈530 eV. The presence of oxygen is also indicated by the O_{KLL} Auger signal at an apparent binding energy of 974 eV. This indicates that the Sb layer is partially oxidized at least at the surface due to the exposure to air during transport of the sample from the MBE chamber to the XPS system. A tiny C1s signal in this spectrum also signals the presence of very small amounts of carbon containing adsorbates such as hydrocarbons on the surface. After annealing the sample at 420 °C (third spectrum from the top), the signals caused by the substrate are visible again, albeit weaker compared to the initial spectrum because of damping by the remaining Sb overlayer. Note, that oxygen is strongly reduced after this annealing step, which manifests itself in the absence of the O_{KLL} Auger signal as well as in the correct ratio between the $Sb3d_{5/2}$ and $Sb3d_{3/2}$ lines of 3:2. From this behavior, we can conclude that it is possible to desorb the Sb oxide formed on top of the Sb overlayers by annealing at around 400 °C, which will become important further below. Finally, annealing of the sample at 470 °C (lowest spectrum in Figure 2) leads to a complete removal of Sb from the surface. At no stage, an intercalation of Sb under the buffer layer was observed by XPS. This means that Sb desorbs before the surface reaches the temperature that is required for the intercalation of Sb under the buffer layer.

Since annealing of the Sb covered samples in UHV leads to an undesirable fast desorption of Sb, further studies were carried out in which the samples were annealed in an Ar atmosphere at a pressure of $p = 1$ bar at a flow rate of $\phi_{Ar} = 0.5$ slm. The analysis of several samples demonstrated that the desorption of Sb was suppressed sufficiently enough to achieve an intercalation of Sb under the buffer layer, with best results obtained at an annealing temperature of $T = 550\,^\circ$C while annealing time was $t = 60$ min. However, as discussed in the following, the oxidation of the Sb layer during transport in air significantly influences the chemical composition of the interface layer.

Figure 3 summarizes results from two experiments. Figure 3a contains C1s spectra before and after the intercalation processes whereas Figure 3b depicts Sb3d spectra. The corresponding fitting parameters of the spectra shown in Figure 3 as well as of the fits shown in the rest of the work are compiled in the supporting information. Before the deposition of Sb, the C1s spectrum (see topmost spectrum of Figure 3a) shows the typical components of SiC(0001) covered with the buffer layer.[14] While the component labeled SiC at 283.75 eV originates from the substrate, the components S1 and S2 at 284.85 and 285.36 eV, respectively, are due to carbon atoms from the $6\sqrt{3}$ and can be attributed to C atoms bound either only within the carbon layer (S2) or not only within the carbon layer but also to the substrate (S1) as shown in Figure 1.[14] A typical spectrum of the Sb3d core level after deposition of Sb on top of the $6\sqrt{3}$ can be seen in Figure 3b (topmost spectrum). In this case, the thickness of the Sb layer was 250 nm. The spectrum consists of two spin-orbit split doublets ($Sb3d_{3/2}$ and $Sb3d_{5/2}$) and one additional O1s component at 530.48 eV which belongs to oxygen bonded to Sb. The doublet component marked Sb^0 with the $Sb3d_{5/2}$ line at 528.23 eV originates from metallic Sb, whereas the second doublet labeled Sb_2O_x with the $Sb3d_{5/2}$ peak

© 2019 The Authors. Published by WILEY-VCH Verlag GmbH & Co. KGaA, Weinheim

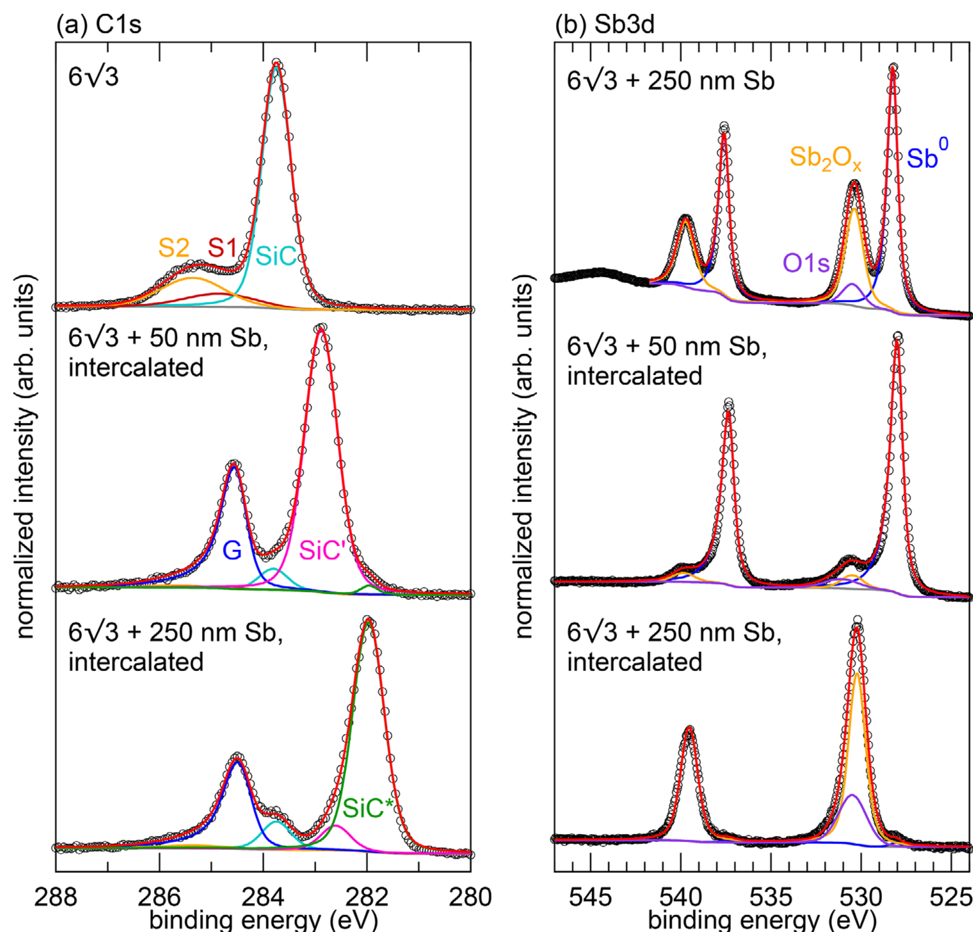

Figure 3. a) XPS spectra of the C1s core level of a pristine $6\sqrt{3}$ sample and of two samples after the intercalation of Sb in Ar atmosphere. b) XPS spectra of the Sb3d core level of a $6\sqrt{3}$ sample covered with 250 nm Sb and of two samples after the intercalation process. Spectra are offset from each other for clarity.

at 530.37 eV belongs to oxidized Sb.[29,30] Similar spectra were observed for all samples after deposition of Sb indicating again the superficial oxidation of the Sb layer during transport in air.

The C1s core levels after the intercalation process are also shown in Figure 3a for a $6\sqrt{3}$ sample initially covered with 50 nm Sb (middle spectrum) and for a $6\sqrt{3}$ sample coated with 250 nm Sb (bottom spectrum). The corresponding Sb3d core levels are presented in Figure 3b. The spectra were fitted using several components as discussed in detail below.

Before discussing the spectra, we recall what is observed for hydrogen intercalation.[19,20] In this case, the buffer layer components S1 and S2 disappeared and an asymmetric C1s component due to QFMLG appeared instead. In addition, the SiC bulk component was shifted to lower binding energy due to a change in surface band bending. A similar behavior is expected for Sb intercalation. Inspection of the C1s spectra after annealing shown in Figure 3, however, shows a somewhat different behavior for the two samples discussed here. In the C1s spectrum of both samples, the transformation of the buffer layer into graphene upon intercalation is evident from the appearance of a strong asymmetric peak labeled G at 284.45 eV (50 nm Sb) and at 284.38 eV (250 nm Sb), respectively. The slight difference in position is caused by different doping as will be shown below. The strongest components marked by SiC' at 282.89 eV for the sample initially covered by 50 nm Sb and SiC* at 281.97 eV for the sample initially covered by 250 nm Sb are due to carbon atoms in the SiC bulk. Apparently, the two samples are characterized by different surface band bending. In addition to the strong peaks, additional weaker components are also observed. First of all, both C1s spectra contain a peak at a binding energy corresponding to the SiC bulk peak of the pristine sample prior to intercalation. This indicates that small areas of the samples have not been intercalated. In accordance, the peaks S1 and S2 have also been included in the fit although their intensities are very small. Secondly, the comparison of the C1s spectra also shows the presence of a small component SiC* at 281.96 eV in the sample initially covered by 50 nm Sb and a small component SiC' at 282.61 eV in the sample initially covered by 250 nm Sb. To understand the origin of the two different bulk components SiC' and SiC*, we have to take a look at the corresponding Sb3d spectra in Figure 3b. For the sample initially covered with 50 nm Sb (middle spectrum in Figure 3b), Sb is found predominantly in a metallic state with a $Sb3d_{5/2}$ binding energy of 527.97 eV. Only a small portion of the Sb is present in an oxidized state as

© 2019 The Authors. Published by WILEY-VCH Verlag GmbH & Co. KGaA, Weinheim

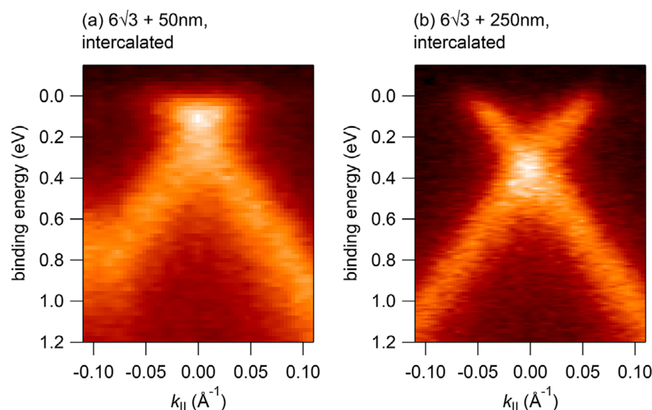

Figure 4. a,b) ARPES measurements near the K point in direction perpendicular to $\overline{\Gamma K}$ of two samples intercalated predominantly with metallic (a) and oxidized (b) Sb. The sample in (a) was coated before the intercalation with 50 nm Sb and the sample in (b) with 250 nm Sb.

can be seen from the rather little component with the Sb3d$_{5/2}$ line at 530.46 eV and the smallish O1s component. On the other hand, the Sb3d spectrum of the sample initially covered by 250 nm Sb, indicates the presence of only small amounts of metallic Sb (Sb3d$_{5/2}$ at 528.07 eV) while most of the Sb is present in the oxidized state (Sb3d$_{5/2}$ at 530.23 eV and O1s at 530.48 eV). We attribute the fact in one case mainly Sb_2O_x, while in other cases mainly metallic Sb was observed after intercalation, to different oxygen contents and different oxygen distributions in the films deposited on the buffer layer. This could be a consequence of, for example, the duration of air exposure prior to intercalation, humidity of the laboratory environment, and the purity/oxygen content of the Sb used as evaporant in the effusion cell. It is plausible that a higher oxygen content deeper in the Sb layer results in a higher oxygen content of the intercalated material.

Taking the observed oxidation state of the intercalated Sb into account, we can conclude that the intercalation of Sb in a metallic state leads to a surface band bending such that the SiC bulk component SiC' is observed while the presence of oxidized Sb at the interface between SiC and graphene leads to a different surface band bending with a SiC bulk component SiC*. The ratio between SiC bulk components (SiC', SiC*) and the graphene component was used to estimate the amount of intercalated Sb. However, due to the fact that the inelastic mean free path in Sb and Sb_2O_x is not very well known, we can only state a range of one to two monolayers. Note, that no C1s components due to defects in the QFMLG were observed which was the case for Bi intercalation via shallow ion implantation.[27]

As mentioned above, the graphene components of the two samples after intercalation G were observed at slightly different binding energies depending on whether the intercalated Sb is metallic or oxidized and it was argued that this is due to different doping. This is readily shown by ARPES. Corresponding measurements close to the K point are shown in **Figure 4**a for the sample initially covered by 50 nm Sb and Figure 4b for the sample with 250 nm Sb. The position of the Dirac point is $E_D - E_F = 0.20$ eV (50 nm Sb) and $E_D - E_F = 0.35$ eV (250 nm Sb), respectively. In both cases, an excess of electrons (n-type doping) by charge transfer from the interface is observed, although the n-type doping by oxidized Sb at the interface is higher than by metallic Sb.

In addition to XPS and ARPES, we characterized the samples by LEED. Typical diffraction images are shown in **Figure 5**. The LEED image of a pristine $6\sqrt{3}$ displays the typical $(6\sqrt{3} \times 6\sqrt{3})R30^\circ$ diffraction pattern as shown in Figure 5a. It presents sharp spots of the SiC and spots of the graphene-like adlayer. All further spots can be explained by superstructure spots from the carbon adlayer covalently bonded to the SiC substrate.[14,31,32] After annealing of the Sb covered $6\sqrt{3}$ in Ar atmosphere, the superstructure spots are strongly suppressed as presented in Figures 5b,c. This indicates a weakening of the bonding to the substrate due to an intercalation of Sb under the $6\sqrt{3}$ accompanied by the formation of QFMLG in good agreement with the XPS results. For the sample intercalated predominantly with metallic Sb shown in Figure 5b, we note that the graphene spots are significantly more intense than the SiC spots. No additional spots are observed which might indicate a lack of long range order in the Sb interlayer. On the other hand, for the sample intercalated predominantly with Sb_2O_x (see Figure 5c) the graphene and SiC spots are of similar intensity. In addition, the superlattice spots are more intense and a significant scattering intensity is observed at the $(\sqrt{3} \times \sqrt{3})R30^\circ$ positions (one example indicated by the red arrow in Figure 5c) which suggests a certain degree of

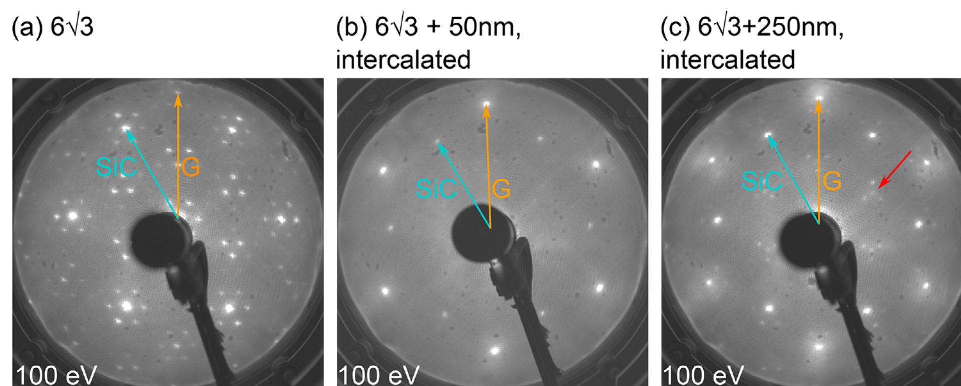

Figure 5. a–c) LEED images of a pristine $6\sqrt{3}$ (a), an intercalated $6\sqrt{3}$ which was coated with 50 nm Sb (b) and 250 nm (c) Sb before the intercalation. In all three images one reciprocal lattice vector of SiC and of graphene (G) is marked.

© 2019 The Authors. Published by WILEY-VCH Verlag GmbH & Co. KGaA, Weinheim

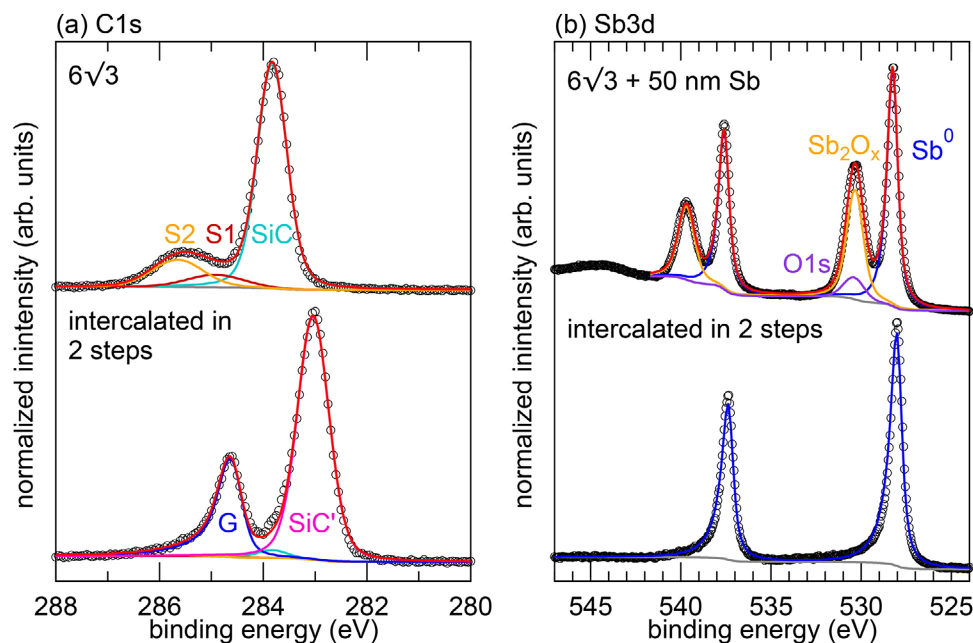

Figure 6. XPS spectra from a sample intercalated by the two-step intercalation process described in the text. a) C1s core level spectra of the $6\sqrt{3}$ sample before (top) and after (bottom) the intercalation of Sb. b) Sb3d spectra of the $6\sqrt{3}$ sample covered with 50 nm Sb before (top) and after (bottom) intercalation. Spectra are offset from each other for clarity.

long range order in the intercalation layer. However, proposing a detailed structural model based on the available data would be too speculative.

As discussed in detail above, annealing of Sb-covered $6\sqrt{3}$ samples in Ar leads to an intercalation of Sb and subsequent conversion of the buffer layer into graphene. However, the unavoidable oxidation of the Sb overlayer during transport in air causes an at least partially, in some cases almost completely oxidized Sb layer at the interface. In order to obtain a truly metallic Sb layer at the interface, it is necessary to first desorb the oxide from the surface. The above mentioned experiments in which the Sb covered samples were annealed in UHV suggest that mild annealing at $T \approx 400\,^{\circ}\mathrm{C}$ should remove the oxide from the surface. Therefore further experiments were conducted in which the annealing in Ar was divided in two consecutive steps. The aim of the first annealing step at $T = 400\,^{\circ}\mathrm{C}$ for $t = 30$ min was to remove the Sb oxide while the second step at $T = 550\,^{\circ}\mathrm{C}$ for $t = 60$ min was intended to intercalate metallic Sb under the buffer layer. As for the previous samples prepared in Ar, the pressure was $p = 1$ bar at an Ar flow rate of $\phi_{\mathrm{Ar}} =$ 0.5 slm.

XPS results of the two-step process are shown in **Figure 6**. The C1s spectrum of the pristine $6\sqrt{3}$ is depicted in Figure 6a (top spectrum). It is virtually identical to the one in Figure 3a and contains the surface components S1 and S2 and the SiC bulk component. The Sb3d spectrum after deposition of 50 nm Sb and prior to annealing is plotted in Figure 6b (top spectrum). As before, the Sb layer is partially oxidized which is evident from the doublet component marked Sb^0 and Sb_2O_x as well as the O1s component. After the two-step process, the C1s spectrum in Figure 6b (bottom spectrum) shows the component labeled G at 284.53 eV, which demonstrates that the buffer layer was decoupled from the SiC substrate and converted into QFMLG by intercalation of Sb. In agreement with that, the spectrum exhibits the component SiC' at 283.04 eV which belongs to the SiC bulk of surface areas intercalated with metallic Sb. In addition, a very small component is observed at the position of the bulk component (SiC) prior to intercalation. From its intensity, we can conclude that a few percent of the sample is not intercalated, similar to the observations for the one-step process. This behavior can be explained as follows. From previous studies it is known that surface steps act as nucleation sites for graphene (see, for example, ref. [6]). For buffer layer samples this means that steps can be decorated with small patches of MLG. In this areas, the intercalating species has to pass an additional graphene layer in order to reach the interface between SiC and the buffer layer. In the case of H-intercalation of MLG on SiC(0001), that is, graphene on the $6\sqrt{3}$, a higher temperature was needed for intercalation compared to the H-intercalation of the bare $6\sqrt{3}$.[33] Therefore, it seems reasonable to assume that the surface areas giving rise to the small bulk component SiC in the lower spectrum of Figure 6a are regions of MLG near steps of the SiC substrate where no intercalation has occurred. As mentioned above, no C1s components due to defects in the QFMLG were observed. The Sb3d spectrum after intercalation (see Figure 6b, lower spectrum) contains a single spin-orbit split doublet with the $3d_{5/2}$ component at 528.03 eV which is evidence for an intercalation of purely metallic Sb. Apparently, the first annealing step indeed removes the Sb oxide from the surface. Note, however, that this cannot be shown explicitly because the removal of the surface from the furnace after the first step would again lead to a superficial oxidation of the Sb in air.

Figure 7a displays the result of an ARPES measurement near the K-point of the hexagonal Brillouin zone of graphene.

© 2019 The Authors. Published by WILEY-VCH Verlag GmbH & Co. KGaA, Weinheim

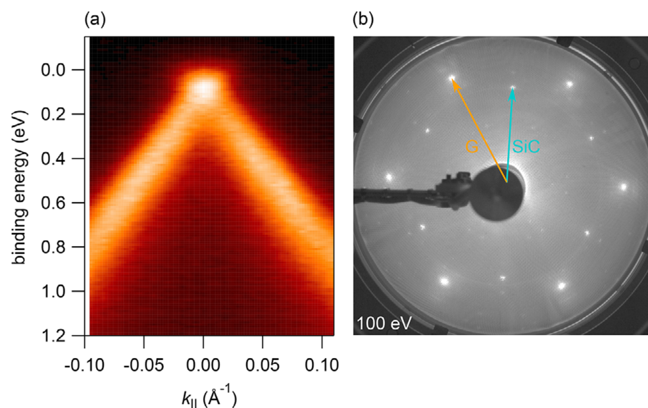

Figure 7. a) ARPES measurement near the K point in direction perpendicular to $\overline{\Gamma K}$ and b) LEED image of a sample intercalated with metallic Sb in the two-step annealing process. In (b) one reciprocal lattice vector of SiC and of graphene (G) is marked.

Relatively sharp π bands are observed with the Dirac point E_D located at 0.09 eV below E_F which corresponds to an electron density of around 0.6×10^{12} cm^{-2}. This is comparable to the results discussed above (see also Table S5, Supporting Information) and indicates that an intercalation with metallic Sb results in small n-type doping. Interestingly, in their intercalation experiments, Niu et al.[34] observed a stronger n-type doping of QFMLG on oxidized Sn (E_D at $\approx$ 0.4 eV) compared to metallic Sn, where the QFMLG was close to neutral. It remains to be seen, however, if this is a general behavior.

A corresponding LEED image is shown in Figure 7b. The LEED image shows diffraction spots from graphene and weaker spots from the SiC(0001) substrate surface. The superstructure spots are strongly suppressed which indicates a reduced interlayer bonding and the transformation of the $6\sqrt{3}$ into QFMLG by intercalation of metallic Sb.

4. Summary and Conclusion

In summary, using XPS, LEED, and ARPES, we have demonstrated that it is possible to intercalate Sb under the $6\sqrt{3}$ on SiC(0001) by annealing of Sb-covered samples in a two-step process in an atmosphere of Ar, which is not possible by annealing in UHV due to the high vapor pressure of Sb. In our process, the Ar atmosphere acts as a buffer and effectively slows down Sb sublimation from the surface such that the temperature necessary for intercalation can be reached. We conclude that the first annealing step at the intermediate temperature leads to the desorption of the Sb_2O_x layer formed on top of the Sb during transport in air. Without this step, the intercalated Sb is at least partially oxidized. Furthermore, we anticipate that a one-step process should suffice if exposure of the Sb-covered samples to air is avoided.

The quasi-freestanding graphene on the Sb interface layer is well ordered and slightly n-type doped with a charge carrier density of 0.6×10^{12} cm^{-2}. No long-range order was observed in the Sb interface layer by LEED. Up to date, it is unclear whether the Sb interlayer is amorphous or if it is comprised of small ordered domains with random orientation. Furthermore, the stability of the intercalation layer with respect to exposure to air and/or temperature should be investigated in future work.

The process introduced here complements other techniques which have been demonstrated for the formation of QFMLG by intercalation under the buffer layer. A schematic representation of several widely used processes is compiled in **Figure 8**. Our Ar-mediated two-step process allows the intercalation of high-vapor-pressure elements which would evaporate from the surface when the sample is annealed in UHV. In comparison with the shallow implantation, which was shown in a previous work by Stöhr et al.[27] for the case of Bi, the deposition of high-vapor-pressure elements like Sb using widely available thermal evaporators is more convenient. In addition, radiation damage

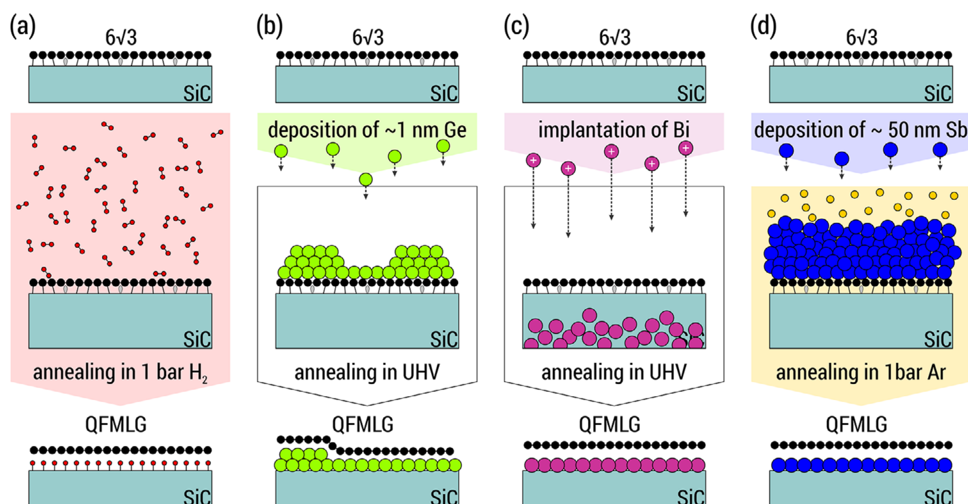

Figure 8. Schematic representation of four different techniques for the preparation of QFMLG by intercalation: a) intercalation of gaseous hydrogen by annealing in H_2 atmosphere,[20] b) intercalation of Ge by deposition and annealing in UHV,[26] c) intercalation of Bi by shallow ion implantation and annealing in UHV,[27] and d) intercalation of high-vapor-pressure Sb by deposition and annealing in Ar atmosphere. Drawing not to scale. No structural or quantitative information should be extracted from the drawing.

© 2019 The Authors. Published by WILEY-VCH Verlag GmbH & Co. KGaA, Weinheim

during implantation, which was observed by Stöhr et al.[27] is avoided. We hope that this stimulates new work on QFMLG on SiC obtained by intercalation of elements which were not accessible by the previously known intercalation recipes.

Supporting Information

Supporting Information is available from the Wiley Online Library or from the author.

Acknowledgements

T.S., F.S., M.W., S.W., and S.R. conceived the experiments; S.W. and S.R. prepared the samples and conducted the experiments with help from F.T., M.V.D., and M.A.; S.W. and S.R analyzed the results with help from F.S., M.W., and T.S.; S.W., T.S., and F.S. wrote the manuscript with input by all other authors; all authors reviewed the manuscript.The research leading to these results was supported by the European Union in the framework of the *Graphene Flagship* under contract no. 696656.

Conflict of Interest

The authors declare no conflict of interest.

Keywords

angle-resolved photoelectron spectroscopy, antimony, buffer layer, epitaxial graphene, intercalation, silicon carbide, X-ray photoelectron spectroscopy

Received: May 13, 2019
Revised: July 10, 2019
Published online: August 22, 2019

[1] K. S. Novoselov, A. K. Geim, S. V. Morozov, D. Jiang, M. I. Katsnelson, I. V. Grigorieva, S. V. Dubonos, A. A. Firsov, *Nature* **2005**, *438*, 197.
[2] C. Berger, Z. M. Song, T. B. Li, X. B. Li, A. Y. Ogbazghi, R. Feng, Z. T. Dai, A. N. Marchenkov, E. H. Conrad, P. N. First, W. A. de Heer, *J. Phys. Chem. B* **2004**, *108*, 19912.
[3] C. Berger, Z. M. Song, X. B. Li, X. S. Wu, N. Brown, C. Naud, D. Mayo, T. B. Li, J. Hass, A. N. Marchenkov, E. H. Conrad, P. N. First, W. A. de Heer, *Science* **2006**, *312*, 1191.
[4] A. J. Van Bommel, J. E. Crombeen, A. Van Tooren, *Surf. Sci.* **1975**, *48*, 463.
[5] P. N. First, W. A. de Heer, T. Seyller, C. Berger, J. A. Stroscio, J. S. Moon, *MRS Bull.* **2010**, *35*, 296.
[6] K. V. Emtsev, A. Bostwick, K. Horn, J. Jobst, G. L. Kellogg, L. Ley, J. L. McChesney, T. Ohta, S. A. Reshanov, J. Roehrl, E. Rotenberg, A. K. Schmid, D. Waldmann, H. B. Weber, T. Seyller, *Nat. Mater.* **2009**, *8*, 203.
[7] C. Virojanadara, M. Syväjarvi, R. Yakimova, L. I. Johansson, A. A. Zakharov, T. Balasubramanian, *Phys. Rev. B* **2008**, *78*, 245403.
[8] M. Kruskopf, D. M. Pakdehi, K. Pierz, S. Wundrack, R. Stosch, T. Dziomba, M. Götz, J. Baringhaus, J. Aprojanz, C. Tegenkamp, J. Lidzba, T. Seyller, F. Hohls, F. J. Ahlers, H. W. Schumacher, *2D Mater.* **2016**, *3*, 041002.
[9] A. Tzalenchuk, S. Lara-Avila, A. Kalaboukhov, S. Paolillo, M. Syväjärvi, R. Yakimova, O. Kazakova, T. J. B. M. Janssen, V. Fal'ko, S. Kubatkin, *Nat. Nanotechnol.* **2010**, *5*, 186.
[10] Y. M. Lin, K. A. Jenkins, A. Valdes-Garcia, J. P. Small, D. B. Farmer, P. Avouris, *Nano Lett.* **2009**, *9*, 422.
[11] Y. M. Lin, C. Dimitrakopoulos, K. A. Jenkins, D. B. Farmer, H. Y. Chiu, A. Grill, P. Avouris, *Science* **2010**, *327*, 662.
[12] Y. M. Lin, A. Valdes-Garcia, S. J. Han, D. B. Farmer, I. Meric, Y. Sun, Y. Wu, C. Dimitrakopoulos, A. Grill, P. Avouris, K. A. Jenkins, *Science* **2011**, *332*, 1294.
[13] A. Mattausch, O. Pankratov, *Phys. Rev. Lett.* **2007**, *99*, 076802.
[14] K. V. Emtsev, F. Speck, T. Seyller, L. Ley, J. D. Riley, *Phys. Rev. B* **2008**, *77*, 155303.
[15] J. B. Hannon, M. Copel, R. M. Tromp, *Phys. Rev. Lett.* **2011**, *107*, 166101.
[16] T. Ohta, A. Bostwick, J. L. McChesney, T. Seyller, K. Horn, E. Rotenberg, *Phys. Rev. Lett.* **2007**, *98*, 206802.
[17] S. Kopylov, A. Tzalenchuk, S. Kubatkin, V. I. Fal'ko, *Appl. Phys. Lett.* **2010**, *97*, 112109.
[18] J. Ristein, S. Mammadov, T. Seyller, *Phys. Rev. Lett.* **2012**, *108*, 246104.
[19] F. Speck, J. Jobst, F. Fromm, M. Ostler, D. Waldmann, M. Hundhausen, H. B. Weber, T. Seyller, *Appl. Phys. Lett.* **2011**, *99*, 122106.
[20] C. Riedl, C. Coletti, T. Iwasaki, A. A. Zakharov, U. Starke, *Phys. Rev. Lett.* **2009**, *103*, 246804.
[21] S. Oida, F. R. McFeely, J. B. Hannon, R. M. Tromp, M. Copel, Z. Chen, Y. Sun, D. B. Farmer, J. Yurkas, *Phys. Rev. B* **2010**, *82*, 041411.
[22] M. H. Oliveira, T. Schumann, F. Fromm, R. Koch, M. Ostler, M. Ramsteiner, T. Seyller, J. M. J. Lopes, H. Riechert, *Carbon* **2013**, *52*, 83.
[23] K. S. Kim, G. H. Park. H. Fukidome, S. Takashi, I. Takushi, K. Fumio, M. Iwao, M. Suemitsu, *Carbon* **2018**, *130*, 792.
[24] I. Gierz, T. Suzuki, R. T. Weitz, D. S. Lee, B. Krauss, C. Riedl, U. Starke, H. Höchst, J. H. Smet, C. R. Ast, K. Kern, *Phys. Rev. Lett.* **2010**, *81*, 235408.
[25] S. Forti, A. Stöhr, A. A. Zakharov, C. Coletti, K. V. Emtsev, U. Starke, *2D Mater.* **2016**, *3*, 035003.
[26] K. V. Emtsev, A. A. Zakharov, C. Coletti, S. Forti, U. Starke, *Phys. Rev. B* **2011**, *84*, 125423.
[27] A. Stöhr, S. Forti, S. Link, A. A. Zakharov, K. Kern, U. Starke, H. M. Benia, *Phys. Rev. B* **2016**, *94*, 085431.
[28] M. Ostler, F. Speck, M. Gick, T. Seyller, *Phys. Status Solidi B* **2010**, *247*, 2924.
[29] F. Garbassi, *Surf. Interface Anal.* **1980**, *2*, 165.
[30] R. Izquierdo, E. Sacher, A. Yelon, *Appl. Surf. Sci.* **1989**, *40*, 175.
[31] C. Riedl, C. Coletti, U. Starke, *J. Phys. D: Appl. Phys.* **2010**, *43*, 374009.
[32] S. Forti, U. Starke, *J. Phys. D: Appl. Phys.* **2014**, *47*, 094013.
[33] S. Mammadov, J. Ristein, R. J. Koch, M. Ostler, C. Raidel, M. Wanke, R. Vasiliauskas, R. Yakimova, T. Seyller, *2D Mater.* **2014**, *1*, 035003.
[34] Y. R. Niu, A. A. Zakharov, R. Yakimova, *Ultramicroscopy* **2017**, *183*, 49.

© 2019 The Authors. Published by WILEY-VCH Verlag GmbH & Co. KGaA, Weinheim